Title

Characterizing the general chelating affinity of serum protein fetuin for lanthanides

Journal

JBIC Journal of Biological Inorganic Chemistry, 25(7)

ISSN

0949-8257

Authors

Pallares, Roger M
Panyala, Nagender R
Sturzbecher-Hoehne, Manuel
et al.

Publication Date

2020-10-01

DOI

10.1007/s00775-020-01815-x

Peer reviewed

Characterizing the General Chelating Affinity of Serum Protein Fetuin for Lanthanides

Roger M. Pallares,[†] Nagender R. Panyala,[†] Manuel Sturzbecher-Hoehne,[†] Marie-Claire Illy,[†] and Rebecca J. Abergel[*†§]

[†]Chemical Sciences Division, Lawrence Berkeley National Laboratory, Berkeley, CA, 94720, USA.

[§]Department of Nuclear Engineering, University of California, Berkeley, CA, 94720, USA

*E-mail: abergel@berkeley.edu

ORCID

Roger M. Pallares: 0000-0001-7423-8706

Rebecca J. Abergel: 0000-0002-3906-8761

ABSTRACT

Fetuin is an abundant blood protein that participates in multiple biological processes, including the transport and regulation of calcium. Fetuin is also known to have a high affinity for uranium (as the uranyl dioxo cation) and plutonium, thus it has been suggested as one of the main endogenous chelating biomolecules involved in the transport of actinides following an internal uptake event. Nevertheless, no direct measurements of its affinity for f-elements beside these two actinides have been reported. Here we investigate the interaction between fetuin and trivalent lanthanides, such as samarium, europium, terbium, and dysprosium, by mass spectrometry and fluorescence spectroscopy. Mass spectrometry results indicated that fetuin has four metal binding sites for the metal ions studied. Upon formation, the metal-protein complexes showed luminescence emission as a result of antenna sensitization of the metal ions, whose photophysics were characterized and exploited to perform direct spectrofluorimetric titrations. Furthermore, the thermodynamic constants were calculated for all complexes, confirming the formation of stable complexes with log β_4' between 26 and 27. In characterizing the affinity of the serum protein fetuin for several f-elements, this study expands upon the initial findings focused on uranyl and plutonium, and contributes to a better understanding of the internal distribution and deposition of lanthanides.

KEYWORDS: Fetuin, lanthanides, luminescence, mass spectrometry

INTRODUCTION

The potential release of toxic radionuclides to the environment as a consequence of industrial activities, such as the processing of nuclear fuel and waste, and accidents in nuclear plants, is considered an important public health and environmental issue [1]. The radionuclides generated during such nuclear-centric activities stem largely from the f-block, including lanthanide (Ln) fission products and actinides (An) [2-4]. Although exposure to these radionuclides has been associated with the development of several pathologies, the biological pathways and biochemical mechanisms involved after internal contamination with most f-elements is still not well understood [5,6]. Although Ln ions do not participate in fundamental biological processes in mammalian systems (unlike in some bacteria [7]), they can bind to endogenous proteins involved in the transport of other metal ions [8,9], such as transferrin through binding sites made of tyrosine and aspartic acid [10,11]. Identifying and studying these biological chelating molecules is important for understanding Ln uptake mechanisms and internal transport, and to develop new decontamination treatments.

Of the many different endogenous targets that can bind Ln and An metal ions, fetuin has been identified as one of the most important for uranyl and plutonium ions [12,13]. Fetuin is an abundant blood protein (homolog of human α2HS glycoprotein) in fetal bovine plasma that participates in a wide range of biological processes, including transport and scavenger functions [14]. Since fetuin contains cystatin-line protein domains, it displays a relatively high affinity for calcium and acts as a Ca(II) carrier and tissue calcification inhibitor [14]. Fetuin is also rich in tyrosine and aspartic acid [15], which can potentially bind to the f-block metal cations (**Figure 1**, the protein molecular structure was calculated with Phyre2 [16]). A previous study determined fetuin as the serum protein with the highest affinity for U(VI), and responsible for carrying up to 80% of the U(VI) present in serum [12]. These data suggested fetuin is the major endogenous chelator involved in the biodistribution of U(VI) through blood,

and therefore responsible for its transport and accumulation into the bones. As only the binding with U(VI) and Pu(IV) has been investigated, it is unclear whether fetuin also participates in the binding and distribution of other f-elements, particularly those in different oxidation states.

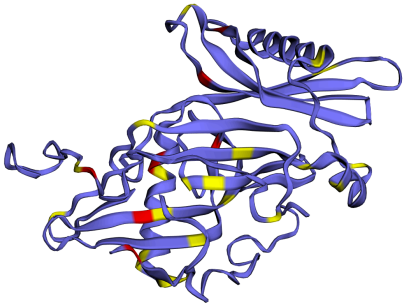

Figure 1. Molecular structure of bovine fetuin-A with tyrosine and aspartate residues highlighted in red and yellow, respectively. The protein structure was calculated with Phyre2 [16].

Here, we investigated the binding characteristics of trivalent samarium, europium, terbium, and dysprosium to the serum protein fetuin. We determined the binding stoichiometry between these f-elements and the protein by mass spectrometry. We also studied the emission of the metal ions through protein antenna sensitization and performed direct spectrofluorimetric titrations, which allowed us to determine the stability constants of the complexes. These results confirmed the formation of stable metal-fetuin complexes, providing further understanding of the interaction between f-elements and endogenous chelators.

RESULTS AND DISCUSSION

Metal complexes of fetuin were initially studied by mass spectrometry (details provided in Experimental Section), a technique commonly used to characterize protein complexes [17]. Four Ln ions (Eu^{3+}, Tb^{3+}, Dy^{3+}, and Sm^{3+}) were selected to start with, based on their unique luminescence properties [18,19]. The mass spectrum of fetuin holo-form was recorded and the number of charges for each peak were assigned (Figure S1). Next, the mass spectra of fetuin complexes formed upon addition of $EuCl_3$ at protein:metal ratio varying from 1:0 to 1:7 were

measured (**Figure 2a**). The spectra changed upon sequential metal addition, indicating the formation of fetuin-Eu complexes, which reached saturation around 1:4 protein:metal ratio. **Figure 2b** shows the peak position for fetuin ions with charge state of -17 upon europium addition, *e.g.* (Fetuin + *i* Eu^{3+} - (17 + *i*)H)$^{17-}$. The same behavior was observed for all tested Ln ions (**Figure 2c**). The peak maxima positions and number of charges were used to determine the molecular weight of the different complexes (Table 1). The number of metal cations bound to the protein was calculated by subtracting the mass of holo-protein to the masses of saturated apo-proteins. In each case, fetuin was found to bind a maximum of four metal ions.

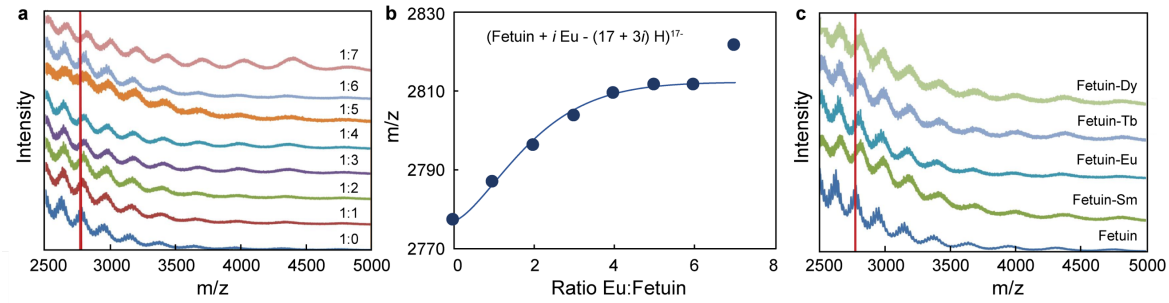

Figure 2. (a) Mass spectra of fetuin (20 μM) with different ratios of Eu(III) at pH 7.4. (b) Variation of fetuin m/z peaks with increasing amount of Eu^{3+}. (c) Representative mass spectra of fetuin (20 μM) with Sm(III), Eu(III), Tb(III), and Dy(III) at fetuin:metal ratio of 1:5. The red line is used as reference to show the shift of the peaks after the addition of lanthanides.

The emission of certain f-block elments can be sensitized by proteins with tyrosine-based binding sites through energy transfer mechanism [11,20]. Hence, the metal sensitization properties of fetuin were explored for the [Fetuin(Ln)$_4$] complexes formed with Sm^{3+}, Eu^{3+}, Tb^{3+}, and Dy^{3+} ions, which are known to emit strong luminescence in the visible through antenna sensitization [18,21-23]. The excitation spectrum of fetuin (Figure S2) shows a band centered at λ_{max} = 280 nm, consistent with other tryptophan-rich proteins [24]; thus the luminescence spectra for all complexes were recorded under excitation at 280 nm. The energy of the fetuin triplet excited state was first determined using the Gd - protein complex (Gd^{3+} ion is similar to Eu^{3+} and Tb^{3+} but lacks an appropriately positioned electronic acceptor level to emit), where the protein phosphorescence was observed through luminescence measurements in a solid matrix (1:3 (v:v) MeOH:EtOH) at 77 K [25]. Gd^{3+} complex showed no luminescence

Table 1. Molecular weight and binding stoichiometry of fetuin-lanthanide complexes determined from mass spectrometry data.

	Total Mass (Da)	**Δ Mass (Da)**	**Metal:Protein**
Fetuin	48942 ± 3874		
Fetuin-Sm	49611 ± 3891	669 ± 22	4.2 ± 0.1
Fetuin-Eu	49506 ± 3845	559 ± 60	3.7 ± 0.4
Fetuin-Tb	49627 ± 3895	680 ± 35	4.3 ± 0.2
Fetuin-Dy	49616 ± 3881	669 ± 37	4.1 ± 0.2

from 400 to 450 nm at room temperature but, upon cooling to 77 K, an intense phosphorescence with vibrational structure was recorded (Figure S3), which is characteristic of phosphorescence from a tryptophan-containing protein triplet excited state [26,27]. From the positions of the highest band, the energy of the lowest T_1 excited state was calculated at 22,831 cm^{-1}. The spectra also revealed a broad fluorescence band with a maximum of 316 nm, corresponding to a S_1 excited state energy of 31,645 cm^{-1}, and consistent with other tryptophan-rich proteins [28]. Based on these singlet and triplet excited state values, fetuin was expected to sensitize the luminescence of Sm^{3+}, Eu^{3+}, Tb^{3+}, and Dy^{3+}, since (1) antenna sensitization frequently occurs as energy transfer from the ligand lowest triplet state to the Ln lowest excited level, and (2) the triplet excited state of fetuin was higher in energy than the lowest emitting state of each metal [29].

Sensitized emission was indeed observed in the visible range for the metal-protein complexes (**Figure 3**) with emission peaks at $\lambda_{em}(Sm^{3+})$ = 595, 645, 703 nm; $\lambda_{em}(Eu^{3+})$ = 588,

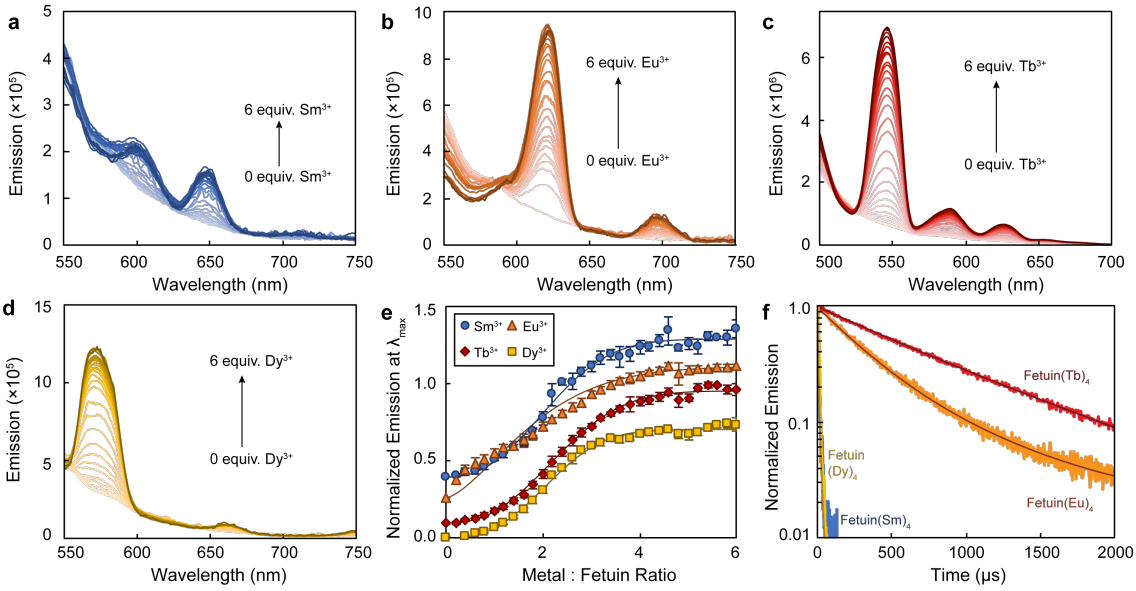

Figure 3. Emission of fetuin complexes after the addition of different equivalents of (a) Sm^{3+}, (b) Eu^{3+}, (c) Tb^{3+}, and (d) Dy^{3+} at pH 7.4. The concentration of fetuin was 150 μM. (e) Normalized emission at 645, 615, 545, and 572 nm for Sm^{3+}, Eu^{3+}, Tb^{3+}, and Dy^{3+}. The curves have been offset for clarity. (f) Time-resolved luminescence of the different saturated fetuin-metal complexes at pH 7.4. The solid dark lines represent the fitting with reduced chi-square (χ^2_ν) of 1.15, 1.14, 1.12, and 1.19 for the Sm^{3+}, Eu^{3+}, Tb^{3+}, and Dy^{3+} complexes, respectively. The excitation wavelength for all experiments was 280 nm.

615, 649, 694 nm; $\lambda_{em}(Tb^{3+})$ = 545, 586, 620 nm; $\lambda_{em}(Dy^{3+})$ = 572, 660 nm. The luminescence quantum yields of the four [Fetuin(Ln)$_4$] complexes were determined with the optical dilution method (Figure S4). Solutions were prepared with a 1:5 protein:metal ratio in buffered aqueous solutions at pH 7.4 to ensure the formation of the saturated protein complexes. Table 2 reports the quantum yields that decrease in the following order $Tb^{3+} > Eu^{3+} > Dy^{3+} > Sm^{3+}$. Because Tb^{3+} and Dy^{3+} have high metal emitting excited states ($^5D_4$ at 20,500 cm^{-1} for Tb^{3+}, and $^4F_{9/2}$ at 21,100 cm^{-1} for Dy^{3+}) [29], the quantum yield values of their complexes were expected to be affected by energy transfer/back-transfer processes [30]. Time-resolved analysis of the luminescence of the emitting complexes (measured at 645 nm, 615 nm, 545 nm and 572 nm, for Sm^{3+}, Eu^{3+}, Tb^{3+}, and Dy^{3+}, respectively, Figure 3f) revealed bi-exponential decays, with luminescent lifetimes on the order of a few microseconds for the Dy^{3+} and Sm^{3+} complexes, and longer decay times (up to hundreds of μs) for the Eu^{3+} and Tb^{3+} complexes (Table 2). Based on previous reports, the two lifetimes observed for each complex were attributed to two

different inner-sphere hydrations numbers [31]. Applying the empirical equations for f-elements estimated by Kimura *et al.* [32,33], the number of inner sphere water molecules (q) for the Sm^{3+} and Eu^{3+} complexes in the predominant species was determined between 3 and 4. Tb^{3+} and Dy^{3+} complexes were not calculated, since the experimental equations provide unreliable hydration number when there are back-transfer processes involved [34]. The secondary species displayed longer lifetimes in the Sm^{3+} and Eu^{3+} cases, corresponding to a single inner sphere water molecule.

Table 2. Summary of photophysical parameters for fetuin-metal complexes.

	ϕ in H_2O (%)	**τ in H_2O (µs)**	***%*[a]**	***q***
$Fetuin(Sm)_4$	0.001	6.3 ± 0.4 15.9 ± 0.8	78% 21%	3.7 ± 0.2 1.2 ± 0.1
$Fetuin(Eu)_4$	0.02	282.0 ± 6.6 719.0 ± 10.3	72% 28%	3.3 ± 0.1 1.0 ± 0.0
$Fetuin(Tb)_4$	0.1	536.0 ± 17.8 984.1 ± 4.4	39% 61%	
$Fetuin(Dy)_4$	0.004	5.9 ± 0.2 16.3 ± 0.6	85% 15%	

ϕ refers to quantum yield.
τ refers to luminescence lifetimes.
[a] The population of each species was estimated through bi-exponential decay fitting of the time-resolved luminescence data with reduced chi-square (χ^2_ν) of 1.15, 1.14, 1.12, and 1.19 for the Sm^{3+}, Eu^{3+}, Tb^{3+}, and Dy^{3+} complexes, respectively.

The sequential formation constants of the four protein-metal complexes were determined through direct spectrofluorimetric titrations (Figure 3). After the metal addition, the solutions were allowed to reach equilibrium for 60 minutes, until no luminescence change was observed, and the emission spectra recorded (λ_{exc} = 280 nm). The solution emission intensity increased with the concentration of f-element cations, reaching a plateau around 1:4 ratio protein – metal (Figure 3e), consistent with the final ratio determined by mass spectrometry. The fact that both techniques provided the same stoichiometry reinforced the hypothesis that lanthanide luminescence is sensitized in the four binding sites. The titration data consisting of sets of emission spectra with varying concentrations of metal ion were analyzed by nonlinear least-

squares refinements (HypSpec software) [35]. The conditional stepwise binding constants (log K_i') obtained for each metal are summarized in Table 3 and indicate the presence of two sets of two binding sites, one set of two displaying significantly higher affinities (log K_i' values averaging 8.96 ± 0.63) than the other (log K_i' values averaging 4.34 ± 1.46). Of note, we observed several cases, where log K_i' is higher than log K_{i-1}', indicating cooperative binding between the different sites. Both observations, (1) the presence of two sets of binding sites with high and low affinity and (2) the existence of high cooperativity between several binding sites are consistent with a previous report studying the interaction between fetuin and uranyl [12]. The overall conditional binding constants (log β_4') were similar for all the studied cations, averaging at 26.61 ± 0.48, and were comparable to the one previously reported for fetuin – Pu(IV) [13], and the ones published for Eu(III) and Cm(III) with Calmodulin, another calcium-binding protein [36]. Moreover, these overall binding constants were higher than those reported for the complexes formed between these f-elements and the iron-transport protein transferrin [20,37-39]. These data contrast with what was observed and reported for the fetuin complexation of U(VI), as only three binding sites (two with higher affinities than the third one) were evidenced by size exclusion chromatography [12]. These differences can be explained by the different coordination behavior between uranyl (pentagonal equatorial coordination structure [40]) and the trivalent lanthanides (coordination numbers between seven and nine with spherical coordination structures [41]). Finally, although further crystallographic studies are needed to locate fetuin binding sites, trivalent lanthanides are expected to bind to cystatin domain I [15], which is rich of acidic residues (aspartate and glutamate) and tyrosine, known to have high affinity for f-block elements [42].

Table 3. Summary of conditional binding constants for fetuin-metal complexes measured at pH 7.4

	$\log K_1'$	$\log K_2'$	$\log K_3'$	$\log K_4'$	$\log \beta_4'$
Fetuin(Sm)$_i$	8.73 ± 0.20	9.17 ± 0.27	3.55 ± 0.53	5.52 ± 0.53	26.97 ± 0.16
Fetuin(Eu)$_i$	8.55 ± 0.25	8.61 ± 0.27	4.83 ± 0.13	5.00 ± 0.07	26.99 ± 0.05
Fetuin(Tb)$_i$	8.22 ± 0.16	9.94 ± 0.16	5.35 ± 0.05	3.01 ± 0.05	26.52 ± 0.04
Fetuin(Dy)$_i$	8.59 ± 0.11	9.85 ± 0.25	5.84 ± 0.32	1.67 ± 0.31	25.96 ± 0.21
The convergence values (σ) for Sm, Eu, Tb, and Dy complexes were 0.006, 0.013, 0.005, and 0.007, respectively.					

CONCLUSIONS

In summary, we have characterized the binding of different Ln^{3+} metal ions to the serum protein fetuin. Both mass spectrometry and fluorescence spectroscopy indicated that fetuin has four available metal binding sites for the trivalent f-elements studied. In addition, the stepwise and overall binding constants of fetuin with the metal ions were determined using nonlinear least-squares refinements, which confirmed the mass spectrometry and fluorescence spectroscopic results. This study evidences the formation of stable complexes between the protein and trivalent lanthanides, expanding upon the hypothesis put forward by Vidaud and coworkers [12,13] that fetuin is an important endogenous biomolecule involved in the internal transport and distribution of f-element contaminants.

ACKNOWLEDGMENTS

This work was supported by the Laboratory Directed Research and Development Program and by the DOE, Office of Science, Office of Basic Energy Sciences, Chemical Sciences, Geosciences, and Biosciences Division, at the Lawrence Berkeley National Laboratory under Contract DE-AC02-05CH11231.

EXPERIMENTAL SECTION

Materials

All chemicals were obtained from commercial suppliers and were used as received. The Ln^{III} salts utilized were of the highest purity available (>99.9%, Sigma-Aldrich). Metal stock solutions (1 mM) were obtained by dissolving solid $LnCl_3 \cdot nH_2O$ salts in standardized 0.1 M HCl. A Millipore Milli-Q Advantage A10 Water System Production unit was used to purify deionized water.

Sample preparation

Fetuin-A (Sigma-Aldrich) was dissolved in 20 mM HEPES, pH 7.4 for each new sample. Measurements for spectrofluorimetric titration analysis were made at a protein concentration of 150 μM, followed by a time delay for equilibration of 60 min. Fluorescence spectra were recorded with a SpectraMax iD3 Multi-Mode Microplate Reader. Emission data were analyzed by nonlinear regression analysis of fluorescence response versus metal concentration with HypSpec software [35]. Mass spectrometry analysis and photophysical characterization studies were made at a protein concentration of 20 μM in 1 mM NH_4HCO_3, pH 7.4.

Mass spectrometry analysis

Mass spectrometry measurements were performed using an ESI-MS/MSXEVO G2 QTOF system (Waters Technologies) equipped with an electrospray ionization source. The mass spectrometry was performed in negative ion mode because ESI generates more positive ions than negative ones, resulting in “cleaner” spectra with lower background in the negative mode [43]. The ESI source held second electrospray ionization set up for simultaneous injection of the lock-spray resulting in high mass precision measurements. Data acquisition and instrument control were accomplished using the MassLynx software, version 4.1. Samples were directly infused into the ionization chamber from the MS system. The operating parameters were as follows: the nebulization gas flow rate was set to 600 L/h with a desolvation temperature of 300°C, the cone gas flow rate was set to 1 L/h, and the ion source temperature was 100 °C. The

capillary, sample cone, and extraction cone voltage were tuned to 2.00 kV, 80 V, and 4.0 V, respectively. The Q-TOF acquisition rate was 5 s, with a 14 ms inter-scan delay, with an injection flow rate of 5 μL/min. Liquid N_2 served as nebulizer and Ar was used as collision gas. A calibration check of the instrument was performed daily with 0.5 mM CsI, prior to sample analysis. To recalibrate the instrument, a fresh 0.5 mM CsI solution in 2-propanol–water (9:1, v/v) was prepared according to vendor procedures. The sample cone, extraction, and capillary voltages were adjusted to 36 V, 2.5 V and 2.5 kV, respectively. The collision energy was fixed to 22 eV. The recorded mass range was 200-5000 m/z and the calibration mass range was 91.096-5000 m/z by using CsI. The acquired spectra were compared and automatically adjusted to an internal stored reference spectrum. The lock-spray was used to prevent mass shifting over the period of measurements and to correct the acquired spectra. The lock-spray analyte was a 0.1% formic acid solution of 2 ng/L leucin-enkephalin (Waters Corporation, 556.2771 m/z $[M+H]^+$) in acetonitrile–water (1:1, v/v) prepared according to vendor procedures. Leucin Enkephalin was used as an internal standard in the optimization of the mass spectrometers for LC–MS experiments. The instrument was tuned using the standard solution to provide a minimum mass accuracy or resolving power of 22,500 FWHM resolution (full width at half-maximum, m/z 556.2771 $[M+H]^+$ in ESI (+) mode) and a mass error for 11 replicates of 0.6 ppm. This solution was used as a lock mass to correct small mass drifts during multiple measurements. During mass spectrometry acquisitions the lock-spray solution was injected every 30 s for a scan time of 0.1 s, with a flow rate of 10 μL/min. The capillary voltage was set to 3.0 kV and the collision energy to 15 eV.

Characterization of metal-complex photophysical properties

UV-Visible absorption spectra were recorded either on a Varian Cary 300 double beam absorption spectrometer or Ocean Optics USB 4000, using quartz cells with a 1.00 cm path length. Excitation and emission spectra and lifetimes were acquired on a HORIBA Jobin Yvon

IBH FluoroLog-3 spectrofluorimeter, as described elsewhere [44]. Luminescence spectra were followed for the protein emission band between 290-450 nm upon excitation of the absorption maximum of the protein (λ_{exc} = 280 nm) with 5-10 nm slits, while metal emission band were observed in the 500-750 nm range with the slits adjusted to 5-14 nm. Lifetime analysis of fetuin complexed with Eu^{3+}, Tb^{3+}, Dy^{3+} or Sm^{3+} was performed at emission maxima (λ_{max} = 612 (Eu), 545 (Tb), 572 (Dy), 645 nm (Sm)), using the same spectrofluorimetry instrumentation coupled to a Xenon pulsed light source. Goodness of fit was assessed by minimizing the reduced chi squared function, χ^2, and a visual inspection of the weighted residuals. Quantum yields were determined by the optical dilution method, using an excitation wavelength of 280 nm and tyrosine as a reference standard (Φ_r = 0.14) [45]. Procedures for the data treatment of quantum yields and kinetic parameters have been reported elsewhere [25]. The experiments were performed in triplicates and the results reported as the measurement average and one standard deviation.

Titration data treatment

The emission spectra from the titration experiments were recorded with a SpectraMax iD3 Multi-Mode Microplate Reader, and imported into HypSpec software and analyzed by nonlinear least-squares refinement [35]. Conditional equilibrium constants were defined as both stepwise (K') and cumulative formation constants (β') based on the following equations, where metal is described as M:

Stability Constants	**Equilibrium reactions**
$K_1' = \frac{[\mathrm{M\ Fetuin}]}{[\mathrm{M}][\mathrm{Fetuin}]}$	$\mathrm{M} + \mathrm{Fetuin} \rightleftharpoons \mathrm{M\ Fetuin}$
$K_2' = \frac{[\mathrm{M_2Fetuin}]}{[\mathrm{M}][\mathrm{M\ Fetuin}]}$	$\mathrm{M} + \mathrm{M\ Fetuin} \rightleftharpoons \mathrm{M_2Fetuin}$
$K_3' = \frac{[\mathrm{M_3Fetuin}]}{[\mathrm{M}][\mathrm{M_2Fetuin}]}$	$\mathrm{M} + \mathrm{M_2Fetuin} \rightleftharpoons \mathrm{M_3Fetuin}$
$K_4' = \frac{[\mathrm{M_4Fetuin}]}{[\mathrm{M}][\mathrm{M_3Fetuin}]}$	$\mathrm{M} + \mathrm{M_3Fetuin} \rightleftharpoons \mathrm{M_4Fetuin}$

$\beta_4' = \frac{[\mathrm{M_4Fetuin}]}{[\mathrm{M}]^4[\mathrm{Fetuin}]}$	$4\,\mathrm{M} + \mathrm{Fetuin} \rightleftharpoons [\mathrm{M_4Fetuin}]$

The chemical equilibria included in the constant calculations were water autoprotolysis, protein metal complex formation, and metal hydroxide formation. The stability constants used during the refinement process are included in Table S1. The goodness of the fit was assessed by minimizing the convergence value (σ), which is the weighted sum of squares.

Notes

The authors declare no competing financial interest.

REFERENCES

1. Cassatt DR, Kaminski JM, Hatchett RJ, DiCarlo AL, Benjamin JM, Maidment BW (2008) Medical Countermeasures against Nuclear Threats: Radionuclide Decorporation Agents. Radiat Res 170 (4):540-548. doi:10.1667/RR1485.1
2. Ewing RC, Weber WJ (2011) Actinide Waste Forms and Radiation Effects. In: Morss LR, Edelstein NM, Fuger J (eds) The Chemistry of the Actinide and Transactinide Elements. Springer Netherlands, Dordrecht, pp 3813-3887. doi:10.1007/978-94-007-0211-0_35
3. Konings RJM, Wiss T, Guéneau C (2011) Nuclear Fuels. In: Morss LR, Edelstein NM, Fuger J (eds) The Chemistry of the Actinide and Transactinide Elements. Springer Netherlands, Dordrecht, pp 3665-3811. doi:10.1007/978-94-007-0211-0_34
4. Carter KP, Pallares RM, Abergel RJ (2020) Open questions in transplutonium coordination chemistry. Communications Chemistry 3 (1):103. doi:10.1038/s42004-020-00338-5
5. Cardis E, Krewski D, Boniol M, Drozdovitch V, Darby SC, Gilbert ES, Akiba S, Benichou J, Ferlay J, Gandini S, Hill C, Howe G, Kesminiene A, Moser M, Sanchez M, Storm H, Voisin L, Boyle P (2006) Estimates of the cancer burden in Europe from radioactive fallout from the Chernobyl accident. Int J Cancer 119 (6):1224-1235. doi:10.1002/ijc.22037
6. Hasegawa A, Tanigawa K, Ohtsuru A, Yabe H, Maeda M, Shigemura J, Ohira T, Tominaga T, Akashi M, Hirohashi N, Ishikawa T, Kamiya K, Shibuya K, Yamashita S, Chhem RK (2015) Health effects of radiation and other health problems in the aftermath of nuclear accidents, with an emphasis on Fukushima. The Lancet 386 (9992):479-488. doi:https://doi.org/10.1016/S0140-6736(15)61106-0
7. Daumann LJ (2019) Essential and Ubiquitous: The Emergence of Lanthanide Metallobiochemistry. Angewandte Chemie International Edition 58 (37):12795-12802. doi:10.1002/anie.201904090
8. Deblonde GJP, Sturzbecher-Hoehne M, Mason AB, Abergel RJ (2013) Receptor recognition of transferrin bound to lanthanides and actinides: a discriminating step in cellular acquisition of f-block metals. Metallomics 5 (6):619-626. doi:10.1039/C3MT20237B
9. Vincent JB, Love S (2012) The binding and transport of alternative metals by transferrin. Biochimica et Biophysica Acta (BBA) - General Subjects 1820 (3):362-378. doi:https://doi.org/10.1016/j.bbagen.2011.07.003
10. Jeanson A, Ferrand M, Funke H, Hennig C, Moisy P, Solari PL, Vidaud C, Den Auwer C (2010) The Role of Transferrin in Actinide(IV) Uptake: Comparison with Iron(III). Chemistry – A European Journal 16 (4):1378-1387. doi:10.1002/chem.200901209
11. White GF, Litvinenko KL, Meech SR, Andrews DL, Thomson AJ (2004) Multiphoton-excited luminescence of a lanthanide ion in a protein complex: Tb3+ bound to transferrin. Photochem Photobiol Sci 3 (1):47-55. doi:10.1039/B306760B
12. Basset C, Averseng O, Ferron P-J, Richaud N, Hagège A, Pible O, Vidaud C (2013) Revision of the Biodistribution of Uranyl in Serum: Is Fetuin-A the Major Protein Target? Chem Res Toxicol 26 (5):645-653. doi:10.1021/tx400048u
13. Vidaud C, Miccoli L, Brulfert F, Aupiais J (2019) Fetuin exhibits a strong affinity for plutonium and may facilitate its accumulation in the skeleton. Scientific Reports 9 (1):17584. doi:10.1038/s41598-019-53770-6
14. Jahnen-Dechent W, Heiss A, Schäfer C, Ketteler M, Towler Dwight A (2011) Fetuin-A Regulation of Calcified Matrix Metabolism. Circ Res 108 (12):1494-1509. doi:10.1161/CIRCRESAHA.110.234260
15. Dziegielewska KM, Brown WM, Casey SJ, Christie DL, Foreman RC, Hill RM, Saunders NR (1990) The complete cDNA and amino acid sequence of bovine fetuin. Its homology with alpha 2HS glycoprotein and relation to other members of the cystatin superfamily. J Biol Chem 265 (8):4354-4357
16. Kelley LA, Mezulis S, Yates CM, Wass MN, Sternberg MJE (2015) The Phyre2 web portal for protein modeling, prediction and analysis. Nat Protoc 10:845. doi:10.1038/nprot.2015.053

17. Boeri Erba E, Petosa C (2015) The emerging role of native mass spectrometry in characterizing the structure and dynamics of macromolecular complexes. Protein Sci 24 (8):1176-1192. doi:10.1002/pro.2661
18. Hänninen P, Härmä H (2011) Lanthanide luminescence: photophysical, analytical and biological aspects. Springer-Verlag Berlin Heidelberg,
19. Pallares RM, Sturzbecher-Hoehne M, Shivaram NH, Cryan JP, D'Aléo A, Abergel RJ (2020) Two-Photon Antenna Sensitization of Curium: Evidencing Metal-Driven Effects on Absorption Cross Section in f-Element Complexes. The Journal of Physical Chemistry Letters 11 (15):6063-6067. doi:10.1021/acs.jpclett.0c01888
20. Sturzbecher-Hoehne M, Goujon C, Deblonde GJP, Mason AB, Abergel RJ (2013) Sensitizing Curium Luminescence through an Antenna Protein To Investigate Biological Actinide Transport Mechanisms. J Am Chem Soc 135 (7):2676-2683. doi:10.1021/ja310957f
21. Pallares RM, Abergel RJ (2020) Transforming lanthanide and actinide chemistry with nanoparticles. Nanoscale 12 (3):1339-1348. doi:10.1039/C9NR09175K
22. Pallares RM, Carter KP, Zeltmann SE, Tratnjek T, Minor AM, Abergel RJ (2020) Selective Lanthanide Sensing with Gold Nanoparticles and Hydroxypyridinone Chelators. Inorg Chem 59 (3):2030-2036. doi:10.1021/acs.inorgchem.9b03393
23. Pallares RM, An DD, Tewari P, Wang ET, Abergel RJ (2020) Rapid Detection of Gadolinium-Based Contrast Agents in Urine with a Chelated Europium Luminescent Probe. ACS Sensors 5 (5):1281-1286. doi:10.1021/acssensors.0c00615
24. Möller M, Denicola A (2002) Protein tryptophan accessibility studied by fluorescence quenching. Biochem Mol Biol Educ 30 (3):175-178. doi:10.1002/bmb.2002.494030030035
25. Abergel RJ, D'Aléo A, Ng Pak Leung C, Shuh DK, Raymond KN (2009) Using the Antenna Effect as a Spectroscopic Tool: Photophysics and Solution Thermodynamics of the Model Luminescent Hydroxypyridonate Complex [EuIII(3,4,3-LI(1,2-HOPO))]−. Inorg Chem 48 (23):10868-10870. doi:10.1021/ic9013703
26. Cioni P, Strambini GB (2002) Tryptophan phosphorescence and pressure effects on protein structure. Biochimica et Biophysica Acta (BBA) - Protein Structure and Molecular Enzymology 1595 (1):116-130. doi:https://doi.org/10.1016/S0167-4838(01)00339-9
27. Mukherjee M, Ghosh R, Chattopadhyay K, Ghosh S (2016) Stepwise unfolding of a multi-tryptophan protein MPT63 with immunoglobulin-like fold: detection of zone-wise perturbation during guanidine hydrochloride-induced unfolding using phosphorescence spectroscopy. RSC Advances 6 (66):61077-61087. doi:10.1039/C6RA06545G
28. Vivian JT, Callis PR (2001) Mechanisms of Tryptophan Fluorescence Shifts in Proteins. Biophys J 80 (5):2093-2109. doi:https://doi.org/10.1016/S0006-3495(01)76183-8
29. Kimura T, Nagaishi R, Kato Y, Yoshida Z (2001) Luminescence study on solvation of americium(III), curium(III) and several lanthanide(III) ions in nonaqueous and binary mixed solvents. Radiochimica Acta, vol 89. doi:10.1524/ract.2001.89.3.125
30. Latva M, Takalo H, Mukkala V-M, Matachescu C, Rodríguez-Ubis JC, Kankare J (1997) Correlation between the lowest triplet state energy level of the ligand and lanthanide(III) luminescence quantum yield. J Lumin 75 (2):149-169. doi:https://doi.org/10.1016/S0022-2313(97)00113-0
31. Andrews M, Amoroso AJ, Harding LP, Pope SJA (2010) Responsive, di-metallic lanthanide complexes of a piperazine-bridged bis-macrocyclic ligand: modulation of visible luminescence and proton relaxivity. Dalton Trans 39 (14):3407-3411. doi:10.1039/B923988J
32. Zhang P, Kimura T, Yoshida Z (2004) Luminescence Study on the Inner-Sphere Hydration Number of Lanthanide(III) Ions in Neutral Organo-Phosphorus Complexes. Solvent Extr Ion Exch 22 (6):933-945. doi:10.1081/SEI-200037439
33. Kimura T, Choppin GR (1994) Luminescence study on determination of the hydration number of Cm(III). J Alloys Compd 213-214:313-317. doi:https://doi.org/10.1016/0925-8388(94)90921-0

34. Kovacs D, Phipps D, Orthaber A, Borbas KE (2018) Highly luminescent lanthanide complexes sensitised by tertiary amide-linked carbostyril antennae. Dalton Trans 47 (31):10702-10714. doi:10.1039/C8DT01270A
35. Gans P, Sabatini A, Vacca A (1996) Investigation of equilibria in solution. Determination of equilibrium constants with the HYPERQUAD suite of programs. Talanta 43 (10):1739-1753. doi:https://doi.org/10.1016/0039-9140(96)01958-3
36. Drobot B, Schmidt M, Mochizuki Y, Abe T, Okuwaki K, Brulfert F, Falke S, Samsonov SA, Komeiji Y, Betzel C, Stumpf T, Raff J, Tsushima S (2019) Cm3+/Eu3+ induced structural, mechanistic and functional implications for calmodulin. Phys Chem Chem Phys 21 (38):21213-21222. doi:10.1039/C9CP03750K
37. Binsheng Y, Harris WR (1999) UV difference spectra study on the binding of europium ion with apotransferrin. Acta Chim Sin 57:503-509
38. Harris WR, Chen Y (1992) Difference ultraviolet spectroscopic studies on the binding of lanthanides to human serum transferrin. Inorg Chem 31 (24):5001-5006. doi:10.1021/ic00050a017
39. Abdollahi S, Harris WR (2006) Determination of the Binding Constant of Terbium-Transferrin. Iranian Journal of Chemistry and Chemical Engineering (IJCCE) 25 (1):45-52
40. Pemmaraju CD, Copping R, Smiles DE, Shuh DK, Grønbech-Jensen N, Prendergast D, Canning A (2017) Coordination Characteristics of Uranyl BBP Complexes: Insights from an Electronic Structure Analysis. ACS Omega 2 (3):1055-1062. doi:10.1021/acsomega.6b00459
41. Allen PG, Bucher JJ, Shuh DK, Edelstein NM, Craig I (2000) Coordination Chemistry of Trivalent Lanthanide and Actinide Ions in Dilute and Concentrated Chloride Solutions. Inorg Chem 39 (3):595-601. doi:10.1021/ic9905953
42. Kremer C, Torres J, Domínguez S, Mederos A (2005) Structure and thermodynamic stability of lanthanide complexes with amino acids and peptides. Coord Chem Rev 249 (5):567-590. doi:https://doi.org/10.1016/j.ccr.2004.07.004
43. Reactions and analytical methods for amino acids and peptides (1998). In: Elmore DT, Barrett GC (eds) Amino Acids and Peptides. Cambridge University Press, Cambridge, pp 48-90. doi:DOI: 10.1017/CBO9781139163828.005
44. Sturzbecher-Hoehne M, Ng Pak Leung C, D'Aléo A, Kullgren B, Prigent A-L, Shuh DK, Raymond KN, Abergel RJ (2011) 3,4,3-LI(1,2-HOPO): In vitro formation of highly stable lanthanide complexes translates into efficacious in vivoeuropium decorporation. Dalton Trans 40 (33):8340-8346. doi:10.1039/C1DT10840A
45. Chen RF (1967) Fluorescence Quantum Yields of Tryptophan and Tyrosine. Anal Lett 1 (1):35-42. doi:10.1080/00032716708051097